JOURNAL OF MATERIALS SCIENCE 30 (1995) 3944–3953

Low-cycle fatigue behaviour of notched AISI 304 stainless steel specimens

M. R. BAYOUMI*
Mechanical Engineering Department, Faculty of Engineering, Assiut University, Assiut, Egypt

A. K. ABD EL LATIF
Department of Production Engineering and Mechanical Systems Design, King Abdulaziz University, P.O. Box 9027, Jeddah 21413, Saudi Arabia

Low-cyclic fatigue tests were conducted on semi-circle notched and V-notched specimens made of AISI 304 stainless steel. Extensive scanning electron microscopic examination of the fracture surface was also carried out to correlate the microscopic fracture surface features with the macroscopic fatigue loading parameter for this steel. The elastic–plastic fatigue test results indicated a noticeable cyclic hardening phenomenon and also a great influence of the maximum cyclic stress, the mean stress and the notch geometry on both the fatigue life and the fatigue behaviour process. Using careful sensitivity and regression analysis correlations between the macroscopic fatigue parameters on the one hand and the macroscopic and the microscopic fracture surface features on the other, these correlations are presented and clearly documented and discussed for the two notch geometries investigated.

1. Introduction

In low-cycle fatigue, an initial defect-free material will undergo plastic deformation at a stressed surface until the nucleation of a microcrack takes place. Once this microcrack exists, the plasticity will be localized in its vicinity [1, 2]. A study of the fracturing mechanisms in fatigue thus provides a better understanding of the plastic deformation behaviour of materials undergoing cyclic loading. Low-cycle fatigue is a common form of fatigue testing which can be performed using either stress or strain control. The material response can be represented by hysteresis loops of stress amplitude, $\Delta\sigma$, versus strain amplitude, $\Delta\varepsilon$, and in many materials the first few cycles produce unstabilized hysteresis loops which reflect the fluctuation of the Bauschinger effect in strain-control tests; the stress amplitude will either increase because of hardening or decrease because of softening of the material. This is followed by a stage of quasi-stable loops which can be analysed, and several fatigue properties can be determined. Thus the variation in the plastic strain component, $\Delta\varepsilon_p/2$, with the reversal number of cycles to failure, $2N_f$, is given by the Manson–Coffin equation of the form

$$\Delta\varepsilon_p/2 = \varepsilon_f'(2N_f)^c \quad (1)$$

while a similar relationship, known as the Pasquin equation, gives the fatigue strength properties and takes the following form

$$\Delta\sigma/2 = \sigma_f'(2N_f)^b \quad (2)$$

where ε_f' is the fatigue ductility coefficient, c is the fatigue ductility exponent, σ_f' is the fatigue strength coefficient and b is the fatigue strength exponent.

Because the elastic strain amplitude, ε_e, is σ/E, Equation 2 takes the form

$$\Delta\varepsilon_e/2 = (\sigma_f'/2)(2N_f)^b \quad (3)$$

and the total strain amplitude is given by

$$\Delta\varepsilon_t = \Delta\varepsilon_p + \Delta\varepsilon_e \quad (4)$$

Investigations on the effects of increasing length of a tensile hold period on the uniaxial fatigue of types AISI 304 [3] and AISI 316 [4, 5] stainless steel were reported. These investigations had indicated that the isostrain range lines for AISI 304 stainless steel can be represented by a simple power law relation of the form

$$t_f = AN_f^m \quad (5)$$

where A and m are constants for a given strain range, material, temperature and method of loading. If the time to failure, t_f, is expressed as the time spent during the hold periods and the time spent in completing the rest of the cycle, Equation 5 can be solved for the number of cycles to failure for any hold time, t_h, that is repeated during the tensile portion of each cycle. This expression is given as

$$N_f = (1/fA + t_h/A)^{1/(m-1)} \quad (6)$$

where f is the cyclic frequency. Therefore, once the values of A and m have been determined from a

* *Present address*: Department of Production Engineering and Mechanical Systems Design, King Abdulaziz University, P.O. Box 9027, Jeddah 21413, Saudi Arabia.

0022–2461

number of rather short-hold time tests, the number of cycles to failure for longer hold times can be estimated.

Because fatigue fractures account for the vast majority of in-service failures in most engineering structures and components, either as a result of pure mechanical loading or in conjunction with sliding and friction between surfaces, rolling contact between surfaces, aggressive environments (environmentally assisted or corrosion fatigue) or elevated temperatures (creep fatigue). Such progressive fracture of materials by incipient growth of flaws under cyclically varying stresses can be categorized into the following discrete, yet related, phenomena:

(i) initial cyclic damage in the form of cyclic hardening or softening;
(ii) creation of initial microscopic flaws (microcrack initiation);
(iii) coalescence of these microcracks to form an initial fatal flaw (microcrack growth);
(iv) subsequent macroscopic propagation of this flaw (macrocrack growth);
(v) final catastrophic failure or instability.

In engineering terms, the first three stages, involving cyclic deformation and microcrack initiation and growth, are generally classified together as (macro-) crack initiation, implying the formation of an "engineering sized" detectable crack (e.g of the order of several grain diameters in length). Thus in such terms, the total fatigue life, N, can be defined as the number of cycles necessary both to initiate a (macro-)crack, N_i, and to propagate it subcritically until final failure, N_p, i.e.

$$N = N_i + N_p \quad (7)$$

In fatigue design, where data from laboratory sized specimens are used to predict the lifetime of more complex components in service [6], this distinction between initiation and propagation lives can be critical. Conventional approaches to fatigue design involve the use of S–N curves (stress versus number of cycles) representing the total life resulting from a given stress (or strain) amplitude, suitably adjusted to take into account effects of mean stress, effective stress concentrations at notches (using fatigue strength reduction factors or local strain analysis), amplitude loading (using the Palmgren–Miner cumulative damage law or rainflow counting methods), multixail stresses, environmental effects, and so forth [7]. Although based on total life, this approach (which is in widespread use, particularly in the automotive industry) essentially represents design against crack initiation, because near the fatigue limit, especially in smooth specimens, most of the lifetime is spent in the formation of an engineering-sized crack. In procedures for predicting lifetimes such as S–N or low-cycle fatigue (LCF) testing might simulate the initiation and early growth of the fatigue crack within the fully plastic region of the strain field at some stress concentrator.

Thus, the present study comprehensively addressed three points. The first was to establish and study both monotonic and cyclic curves for AISI 304 stainless steel. The second was to investigate the stress concentration effect on low-cycle fatigue life of AISI 304 stainless steel specimens under different conditions of mean stress and notch geometery. The final point was to analyse the fracture surface features using scanning electron microscopy to understand the micromechanisms of fatigue fracture process in AISI 304 stainless steel. Extensive curve fitting and sensitivity analysis were implemented in each step of this study.

2. Experimental procedure

The material chosen to conduct the experimental tests was AISI 304 stainless steel. The chemical composition of this steel expressed in weight per cent of each element is given in Table I, while the metallographic examination for this steel as received is shown in Fig. 1.

Using Instron testing machine with 50 ton capacity, tensile tests were carried out at room temperature with a crosshead speed of 0.5 mm min^{-1} to determine the mechanical properties.

Two different types of notched cylindrical specimens were used throughout this investigation, specifically semi-circle notch and V-notch, which were adopted to study the effect of stress concentrators on fatigue behaviour. The overall geometry and dimensions of these specimens are shown in Fig. 2.

Elastic–plastic low-cyclic fatigue tests were carried out at different conditions of mean stress and specimen notch geometry. All fatigue tests were conducted at stress-control-mode using 50 ton Instron testing machine under a testing frequency of 10 Hz.

Scanning electron microscopy (type Joel JSM T300) was used to analyse the details of the fracture surfaces features. After each fatigue test, fracture surface specimens were prepared and examined in the scanning electron microscope to determine the fatigued area and the fibrous area, as well as the striations and the dimple sizes under different stress concentrations and mean stress conditions.

TABLE I The chemical composition (wt %) of AISI 304 stainless steel

C	Si	Mn	S	Ni	C	Fe
0.07	0.31	1.11	0.34	8.86	18.3	Bal.

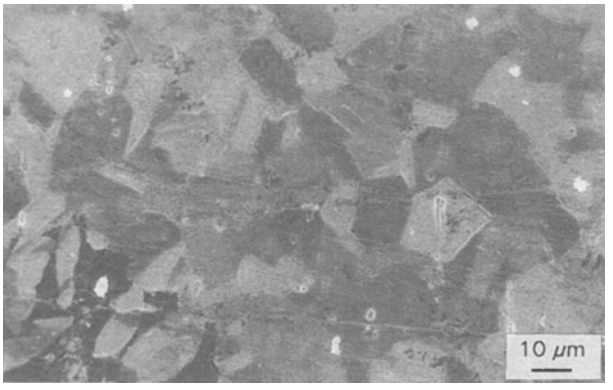

Figure 1 Microstructure of the AISI 304 stainless steel as-received.

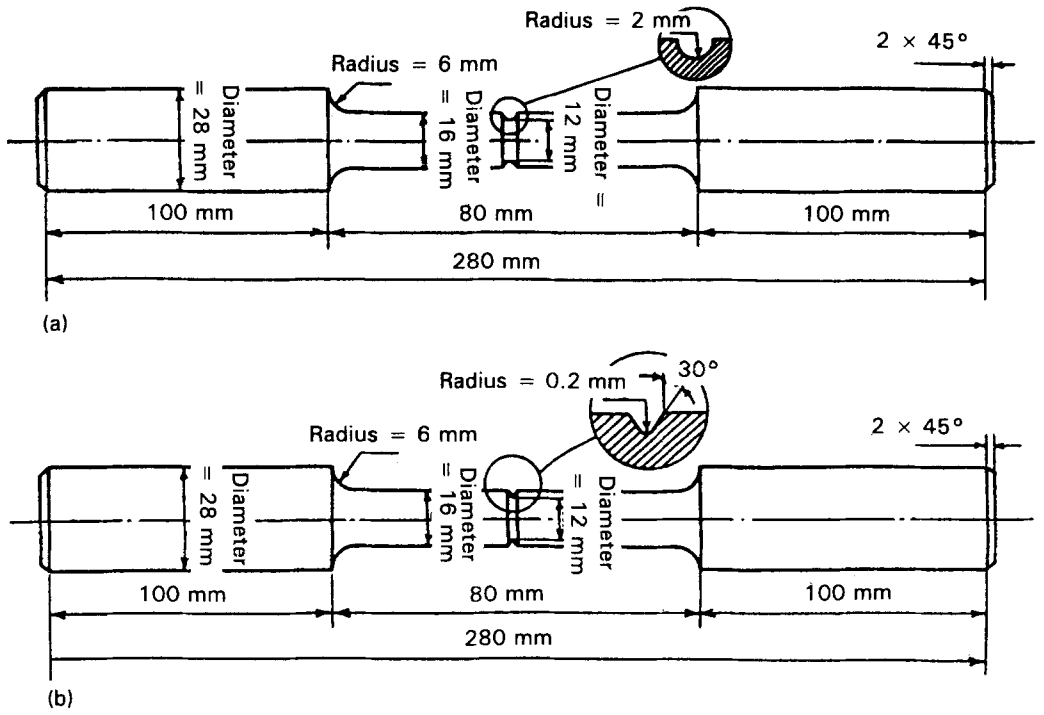

Figure 2 The overall geometry and dimensions of the specimens used in fatigue testing programme.

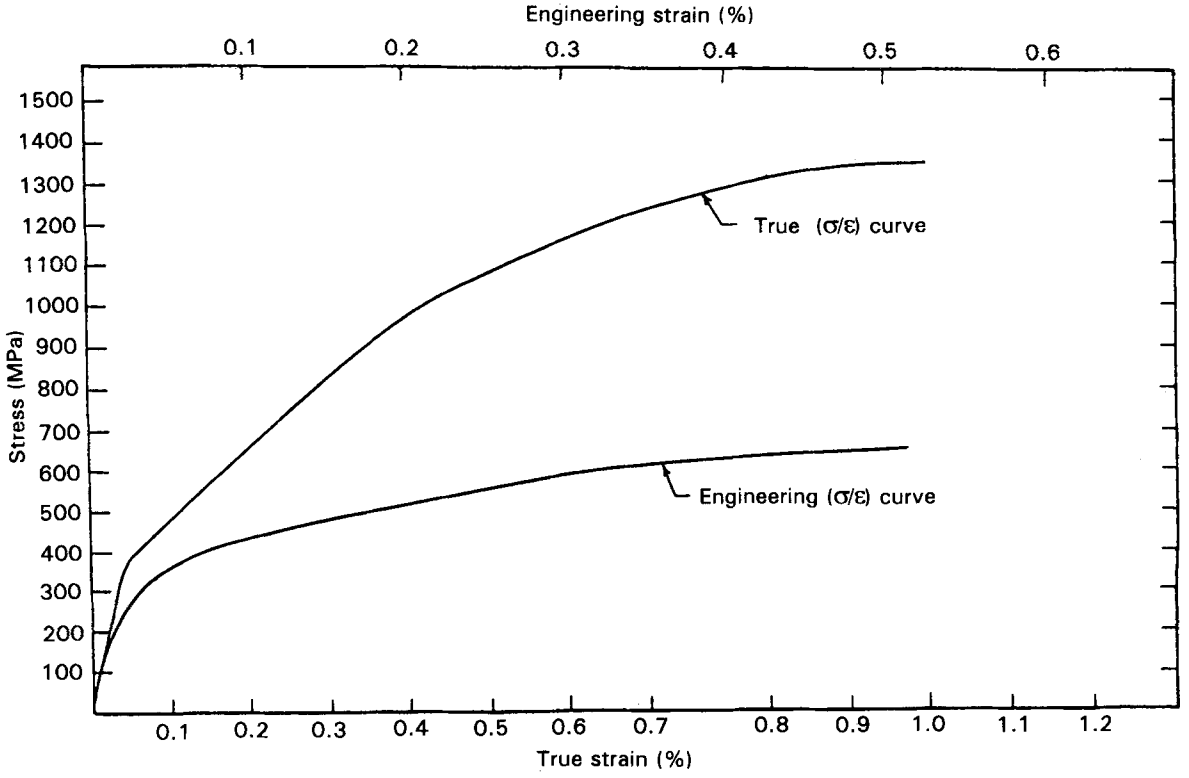

Figure 3 Engineering stress–engineering strain and true stress–true strain diagrams.

3. Results and discussion

The behaviour of the material from tensile tests as expressed in engineering stress versus engineering strain, as well as true stress true strain curves is shown in Fig. 3. The monotonic curve obtained from initial loading of smooth round specimens at different completely reversed strain range and the cyclic stress strain curve of AISI 304 stainless steel obtained by connecting the tips of several hysteresis loops produced during testing of companion specimens at different completely reversed strain range, are presented in Fig. 4. It is clear from this figure that AISI 304 stainless steel possesses a remarkable cyclic hardening phenomena. It can be postulated that the process of hardening is a consequence of the generation of dislocations as well as their clustering and annihilation population. The dislocation population is spontaneously arranged into a characteristic dislocation pat-

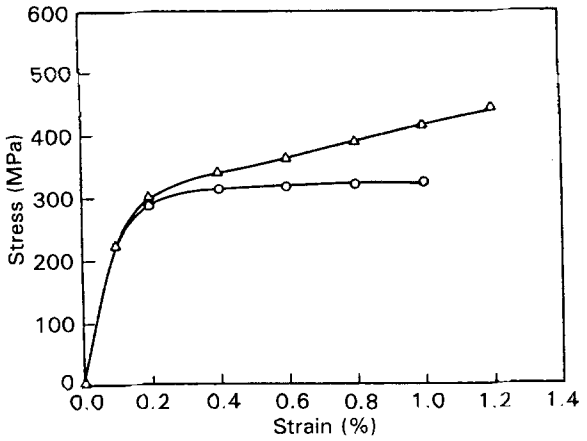

Figure 4 (○) Monotonic and (△) cyclic stress–strain curves for AISI 304 stainless steel.

tern of high and low dislocation density regions [8, 9], where the wavelength and profile of the pattern depends on the applied stress, either uniaxial or cyclic, and change during deformation. Approaching the steady state in the hardening process during deformation is generally accompanied by the annihilation of all the newly generated dislocations in the high-density regions.

The progression of strain with the number of cycles under different values of maximum and minimum cyclic stress levels for both the V-notched and semi-circle notched conditions is presented in Fig. 5. It is clear from this figure that the patterns of the variation of strain with the number of cycles, have two distinct regions with significant deferences in their slopes. If the point of intersection of the average slopes in the two regions is indicated on the number of cycles axes, the number of cycles elapsed from the beginning to this point can be reasonably considered to represent the initiation cycles, N_i, necessary to nucleate cavities or voids, while the remaining life is needed to propagate these cavities or voids to the final separation. Fig. 5 also indicates the large dependence of the nucleation life as discussed earlier, N_i, on the maximum load (maximum stress) as well as the type of notch geometry. It is clearly noticed that for the same life cycles the semi-circle notch withstands significantly higher values of strains than those accompanying the V-notch which emphasizes the influence of both the severity of stress concentration and stress triaxiality effects that are remarkably higher in both magnitude and gradient in the case of the V-notch shape [10, 11]. Furthermore, and based on the previously discussed definition of the initiation life, N_i, and investigating the relationship between this parameter as well as the dependence of the total life to final separation, N_f, on the different testing parameters, specifically the maximum load (maximum stress) and the mean stress for both semi-circle and V-notch, is carefully examined. Thus, Fig. 6a and b show the dependence of N_i and N_f for both semi-circle and V-notch, on the maximum load. It is evident from this figure that both N_i and N_f decrease as the maximum load increases and this decreasing trend for the semi-circle notch is greater than that of the V-notch. This indicates that for the

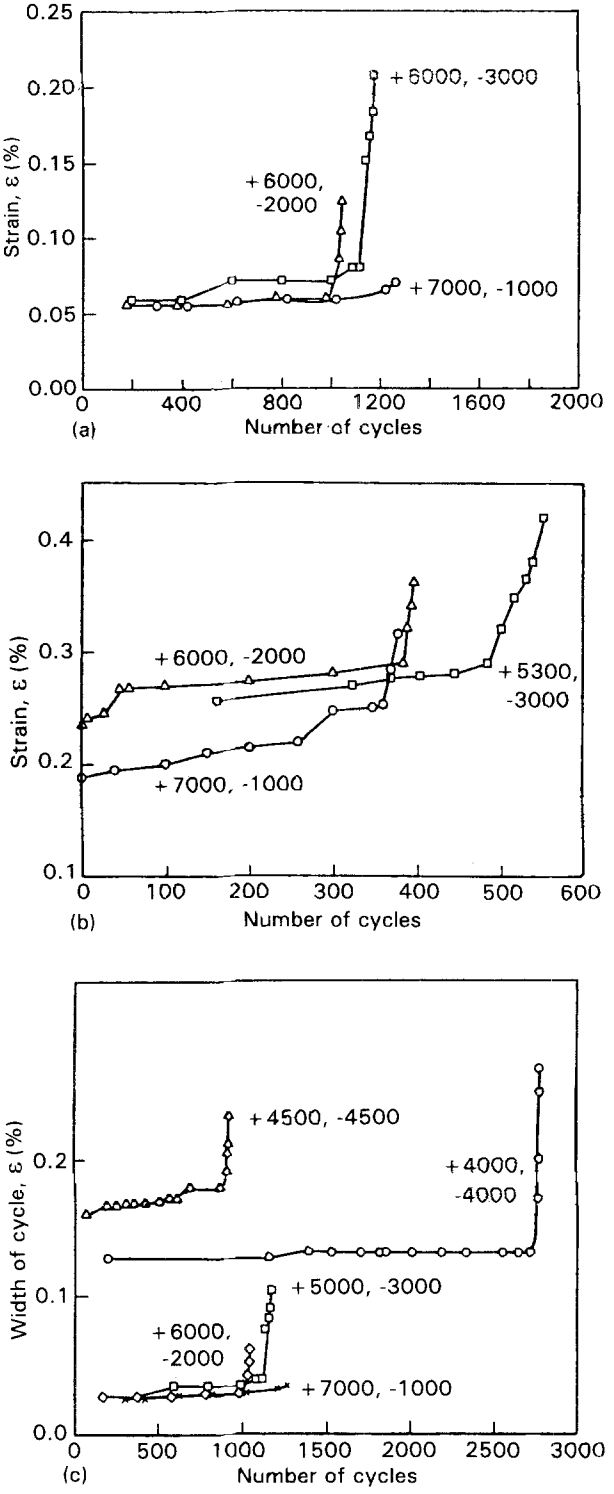

Figure 5 The progression of strain with the number of cycles under different values of maximum and minimum cyclic stress levels, (a) for semi-circle notch at different stress amplitudes; (b) for v-notch at different load amplitudes; (c) for the two notch geometries at different stress amplitudes. (○, △) Semi-circular, (□, ◇, ×) V-notched.

same maximum applied load, the initiation life for the semi-circle configuration is remarkably higher than that of the V-notch configuration. Careful regression analyses were conducted to obtain the quantitative correlations of the dependence of N_i and N_f on the maximum load for both notch geometries. The resulting relationships are presented in Table II.

Because the mean stress, σ_m, is the main macroscopic parameter that has a quite noticeable influence

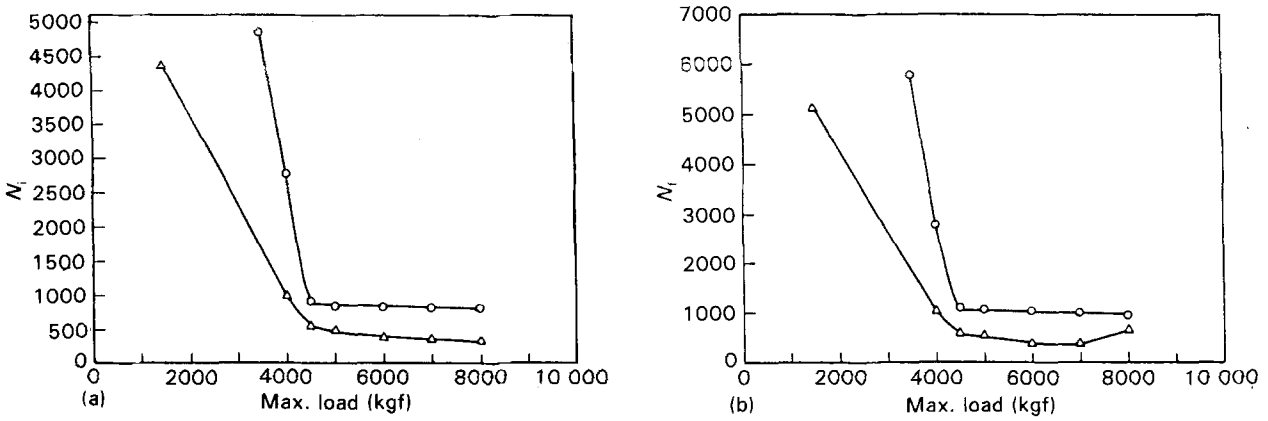

Figure 6 Dependence of the fatigue life stages on the maximum applied cyclic loads for both (○) semi-circle and (△) V-notch specimens. (a) Initiation life, N_i – maximum cyclic load curve; (b) total fatigue life, N_f – maximum cyclic load curve.

TABLE II Correlations between the initiation life, N_i, the total fatigue life, N_f, and the maximum applied cyclic loads, F_{max}, for the two notch geometries

Correlation parameters	Notch geometry	Best regression function	
N_i (cycles) F_{max} (kgf)	(a) Semi-circle	$N_i = 112\,765.476 - 699\,952.5(F_{max}/10\,000) + 1619\,441.37(F_{max}/10\,000)^2$	
		$- 1644\,954.62(F_{max}/10\,000)^3 + 619\,548.56(F_{max}/100\,000)^4$	(8)
	(b) V-notch	$N_i = 7986.849 - 27\,456.72(F_{max}/10\,000) + 18\,368.04(F_{max}/10\,000)^2$	
		$+ 26\,035.86(F_{max}/10\,000)^3 - 26\,320.9(F_{max}/10\,000)^4$	(9)
N_f (cycles) F_{max} (kgf)	(a) Semi-circle	$N_i = 172\,019.76 - 1122\,575.1(F_{max}/10\,000) + 2726\,771.5(F_{max}/10\,000)^2$	
		$- 2904\,830(F_{max}/10\,000)^3 + 1145\,369.5(F_{max}/10\,000)^4$	(10)
	(b) V-notch	$N_f = 11609.367 - 58\,492.48(F_{max}/10\,000) + 116\,536.234(F_{max}/10\,000)^2$	
		$+ 108\,425.63(F_{max}/10\,000)^3 + 40\,953.7(F_{max}/10\,000)^4$	(14)

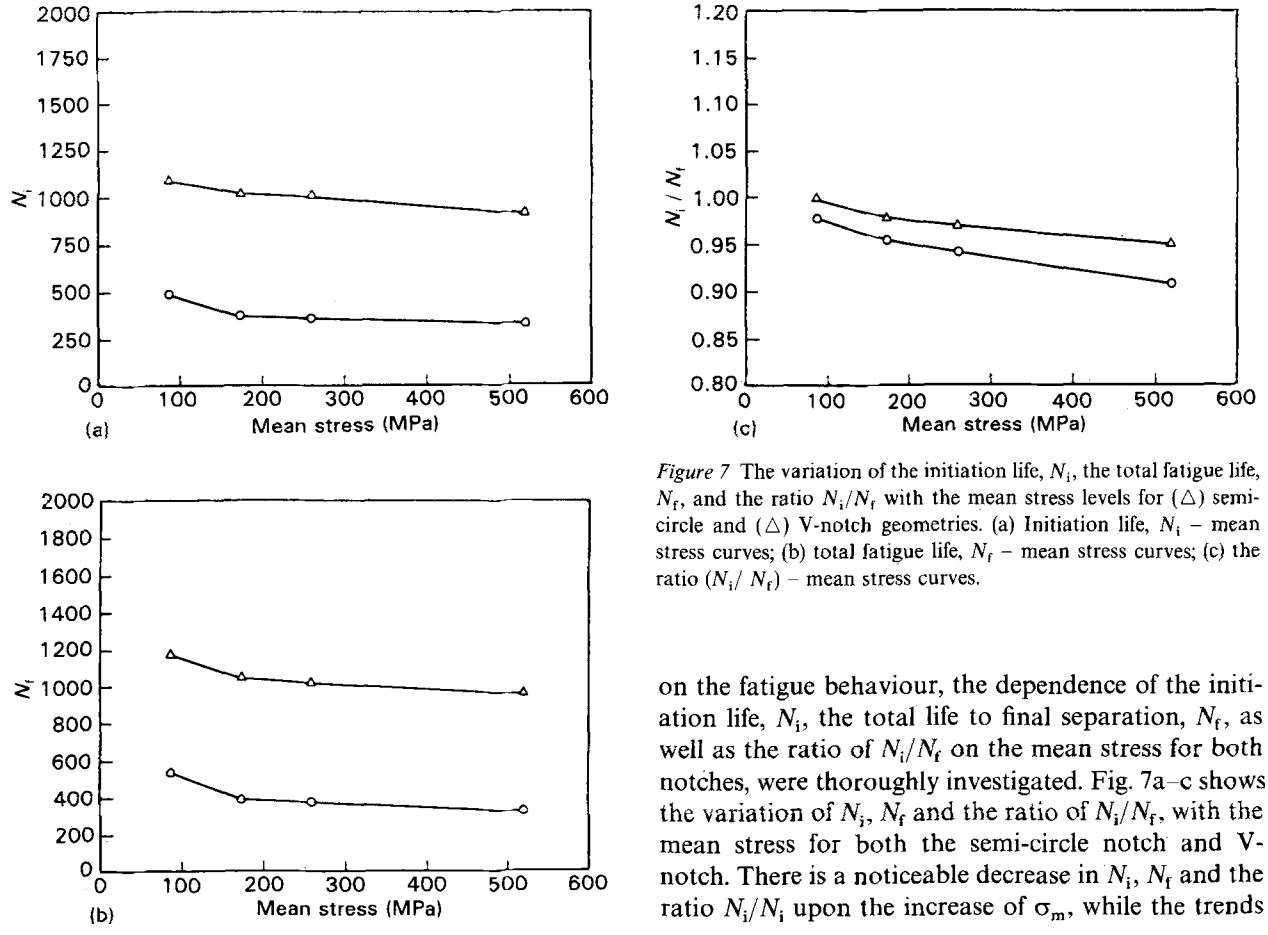

Figure 7 The variation of the initiation life, N_i, the total fatigue life, N_f, and the ratio N_i/N_f with the mean stress levels for (△) semi-circle and (△) V-notch geometries. (a) Initiation life, N_i – mean stress curves; (b) total fatigue life, N_f – mean stress curves; (c) the ratio (N_i/N_f) – mean stress curves.

on the fatigue behaviour, the dependence of the initiation life, N_i, the total life to final separation, N_f, as well as the ratio of N_i/N_f on the mean stress for both notches, were thoroughly investigated. Fig. 7a–c shows the variation of N_i, N_f and the ratio of N_i/N_f, with the mean stress for both the semi-circle notch and V-notch. There is a noticeable decrease in N_i, N_f and the ratio N_i/N_i upon the increase of σ_m, while the trends

for the semi-circle notch are for all parameters remarkably greater than those patterns for the V-notch. The sensitivity and regression analysis was also conducted to obtain the functional relationships of N_i, N_f and N_i/N_f and σ_m, the quantitative correlations for both notch geometries are documented in Table III.

The topography and features of the fracture surfaces of the fatigue specimens were investigated using scanning electron microscopy. Both fracture surfaces from semi-circle and V-notch specimens under different testing conditions were examined. The global characteristic features of all the fatigued surfaces possess two distinct regions, namely the smooth fatigued area which is characterized by beach marks and is dominated by the mechanisms of striation development, and the fibrous area which represents the final separation

TABLE III Dependence of the initiation life, N_i, the total fatigue life, N_f, and the ratio N_i/N_f, on the mean stress, σ_m

Correlation parameters	Notch geometry	Best regression function	
N_i (cycles) σ_m (MPa)	(a) Semi-circle	$N_i = 1260.78 - 1627.91(\sigma_m/600) + 3417.73(\sigma_m/600)^2 - 2311.99(\sigma_m/600)^3$	(12)
	(b) V-notch	$N_i = 763.17 - 2573.42(\sigma_m/600) + 5186.59(\sigma_m/600)^2 - 3219.204(\sigma_m/600)^3$	(13)
N_f (cycles) σ_m (MPa)	(a) Semi-circle	$N_f = 1484.306 - 2892.263(\sigma_m/600) + 5765.7(\sigma_m/600)^2 - 3607.51(\sigma_m/600)^3$	(14)
	(b) V-notch	$N_f = 881.18 - 3219.41(\sigma_m/600) + 6524.83(\sigma_m/600)^2 - 4093.79(\sigma_m/600)^3$	(15)
N_i/N_f σ_m (MPa)	(a) Semi-circle	$N_i/N_f = 1.038\,56 - 0.353\,18(\sigma_m/600) + 0.599\,56(\sigma_m/600)^2 - 0.357\,64(\sigma_m/600)^3$	(16)
	(b) V-notch	$N_i/N_f = 1.0177 - 0.358\,32(\sigma_m/600) + 0.581\,46(\sigma_m/600)^2 - 0.363\,92(\sigma_m/600)^3$	(17)

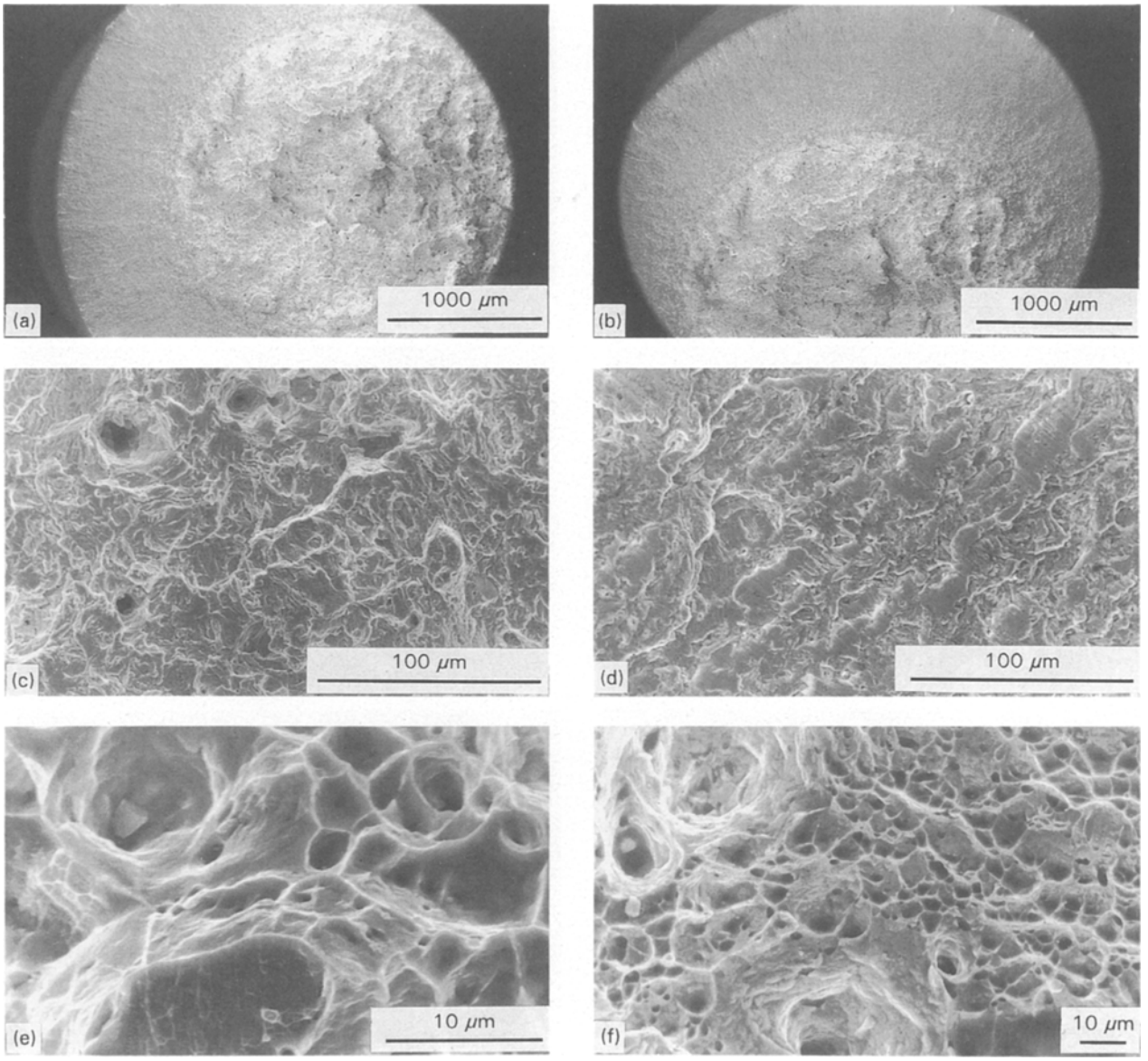

Figure 8 Typical examples of scanning electron micrographs showing (a, b) the overall fracture surface, (c, d) the striations as well the beach marks in the fatigued region, and (e, f) the dimples in the ductile fracture region for the fatigue fractured semi-circle notched specimens. (a, c, d) $F_{max} = +5000$ kgf, $F_{min} = -3000$ kgf. (b, d, f) $F_{max} = +4500$ kgf, $F_{min} = -4500$ kgf.

of the remaining ligament (this area is a ductile fracture region) and is dominated by the nucleation and growth of voids and/or dimples. A semi-analytical approach similar to that reported elsewhere [12, 13], was adopted to determine the size and distribution of dimples for the fracture surfaces of the two notch configurations subjected to different testing conditions. As will be pointed out from the results, the state of strain plays an important role in determining the ratio of the fibrous area to the total area of the fracture surface, the striation width, as well as the relative size, distribution and depth of the voids and/or dimples. All of this resulted in dissimilar topographies of fracture for the semi-circle notched specimens and the V-notched specimens. It is worth mentioning that in the ductile fracture region, the dominant effect of strain in this process is in a global agreement with the mechanics approaches described in the literature [14–16].

Typical examples of the scanning electron micrographs showing the overall fracture surface, the striation as well as the beach marks in the fatigued region, and the dimples in the ductile fracture region, are given in Figs 8 and 9, respectively, for semi-circle notch and V-notch under different cyclic loading conditions. Extensive measurements were taken from these micrographs, namely the ratio of (the equivalent diameter of the fibrous area/the diameter of the total cross-sectional area), striation width (striation spacings) of the fatigued region, as well as the average dimple size and their distribution for each notch under various conditions of the maximum cyclic loads (maximum cyclic stresses) and mean stresses. The relationships between the ratio d/D and the maximum applied cyclic load, as well as the mean stress, is shown in Fig. 10a and b. Increasing either the maximum applied cyclic stress or the mean stress, accompanied by an increase in the remaining ligament area (fibrous area), which means also that the permissible flaw size propagating during the fatigue process decreases upon increasing either the maximum stress or

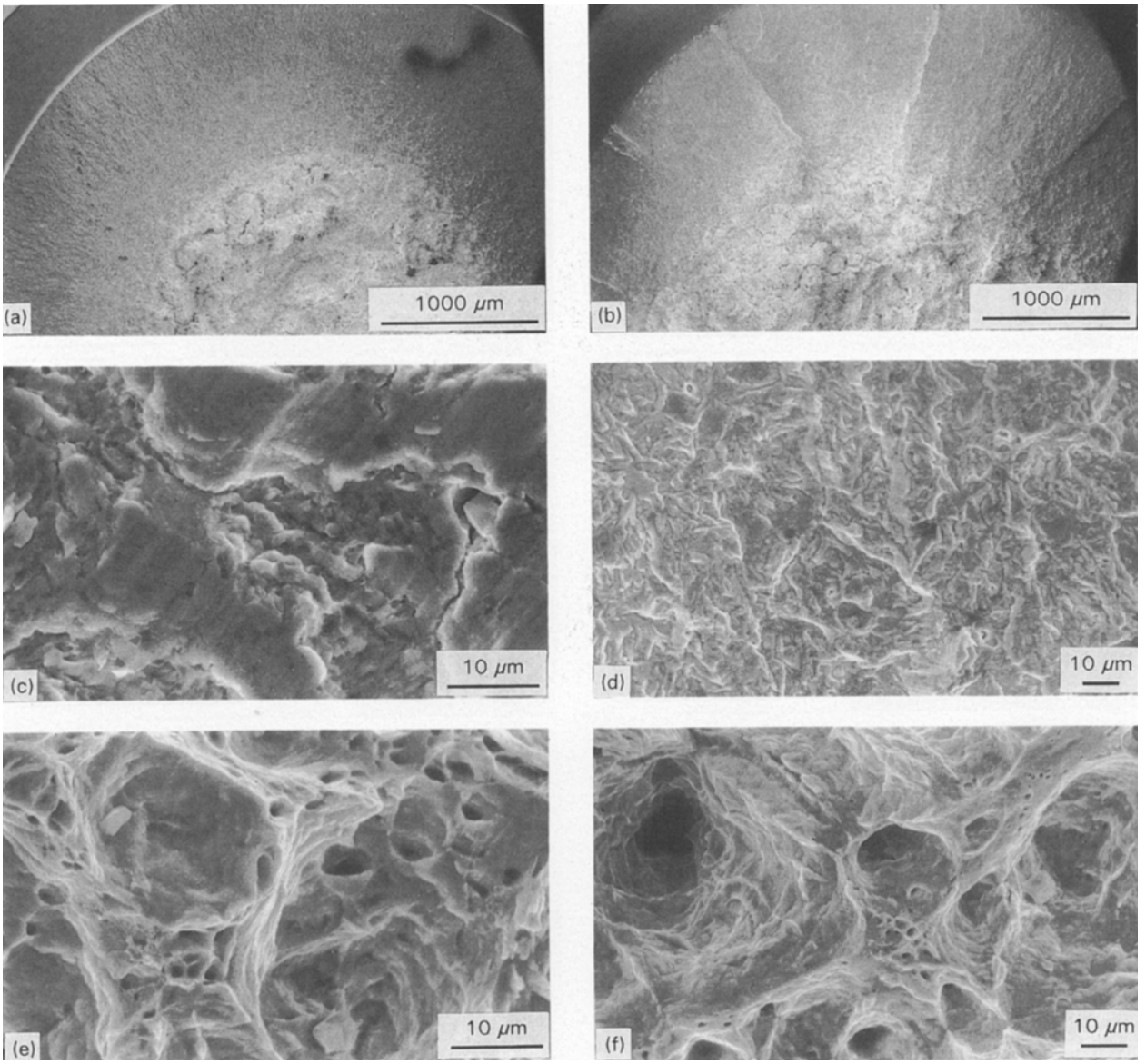

Figure 9 Typical examples of scanning electron micrographs showing (a, b) the overall fracture surface, (c, d) the striations as well as the beach marks in the fatigued region, and (e, f) the dimples in the ductile fracture region for the fatigue fractured V-notched specimens. (a, c, e) F_{max} = + 5000 kgf, F_{min} = − 3000 kgf. (b, d, f) F_{max} = + 4500 kgf, F_{min} = − 4500 kgf.

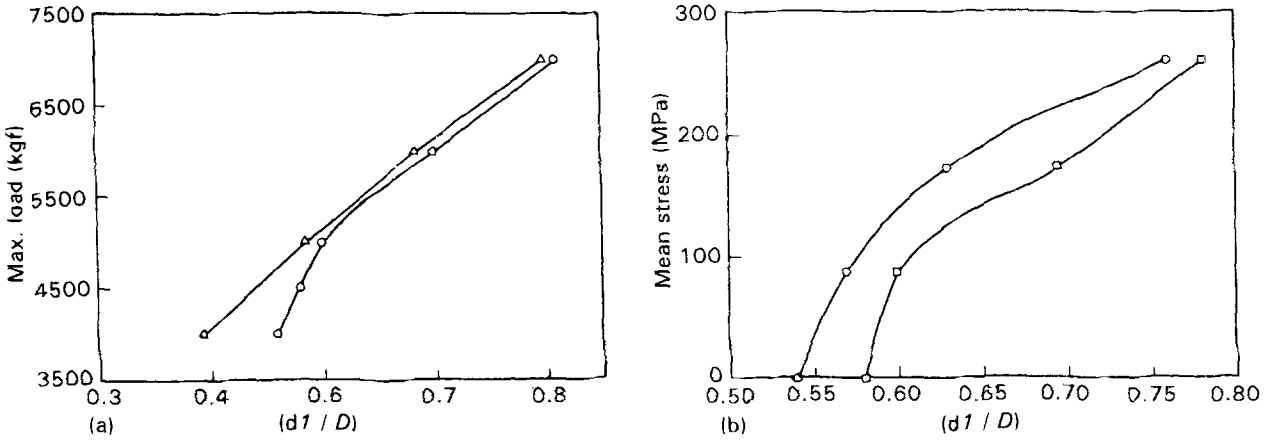

Figure 10 Variation of the ratio of fibrous area diameter, dl, and the total area diameter, D, on the loading parameters for the two notch geometries. (a) Maximum cyclic load–ratio (dl/D) curves; (b) mean stress–ratio (dl/D) curves. (a) (△) semi-circle, (○) V-notch; (b) (○) semi-circle, (△) V-notch.

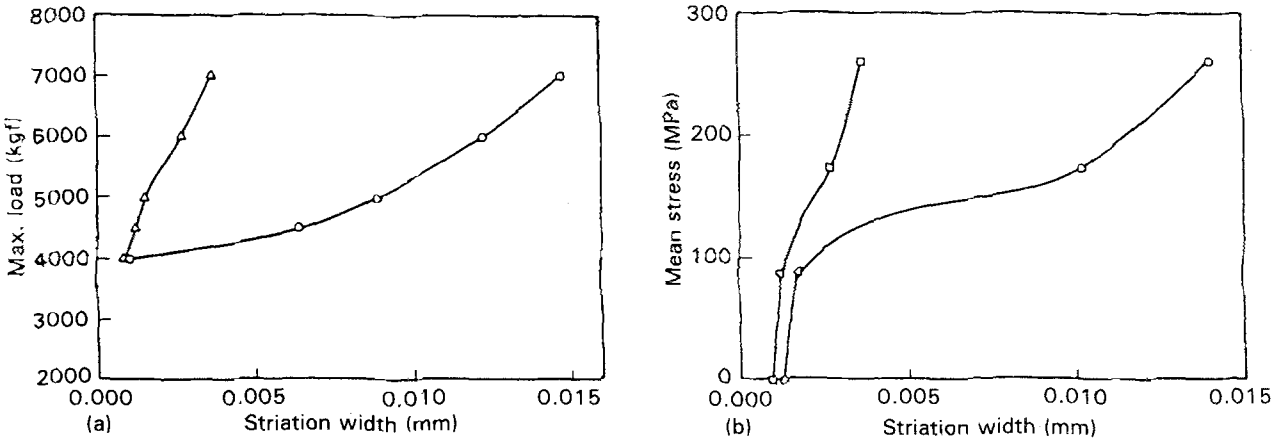

Figure 11 Dependence of the striation width, W, for the two notch geometries, on the maximum cyclic loads as well as the mean stress levels. (a) Maximum load–striation width curves; (b) mean stress–striation width curves. (a) (△) Semi-circle, (○) V-notch. (b) (□) Semi-circle, (○) V-notch.

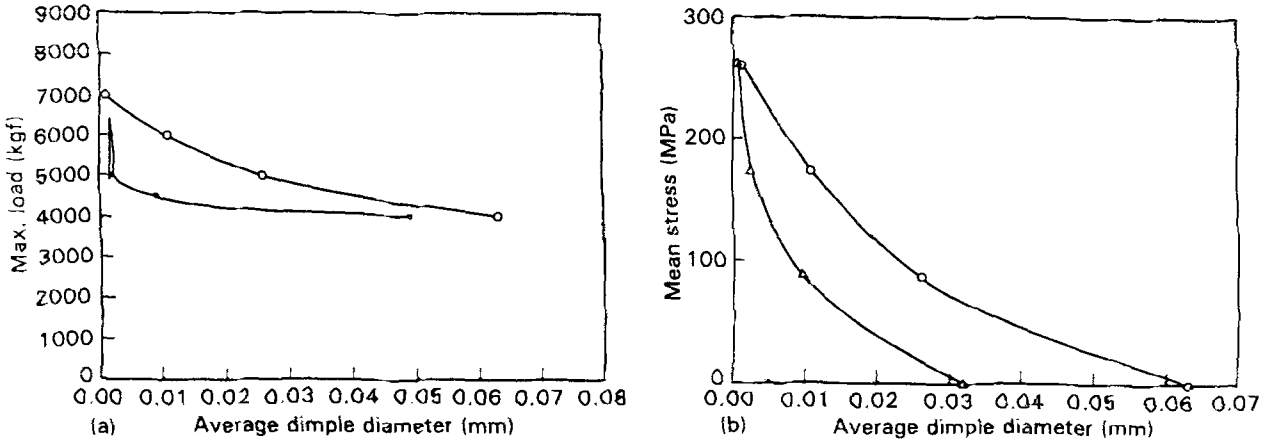

Figure 12 The variation of the average dimple size diameter for the two notch geometries, on the maximum cyclic loads as well as the mean stress levels. (a) Maximum load–average dimple diameter curves; (b) mean stress–average dimple diameter curves. (a) (○) Semi-circle, (●) V-notch. (b) (○) Semi-circle, (△) V-notch.

the mean stress levels. The degree of the change for the semi-circle notch is greater than that of the V-notch. The dependence of the striation width on the maximum cyclic loads, as well as the mean stress values, is presented in Fig. 11a and b. Generally either the maximum cyclic stress or the mean stress causes a significant increase in the striation spacings for both notches, but the amount of increase in the striation width at any specific loading condition is noticeably less for the semi-circle notch than that of the V-notch, especially at higher levels of either the maximum or mean stresses. The dependence of the ductile fracture

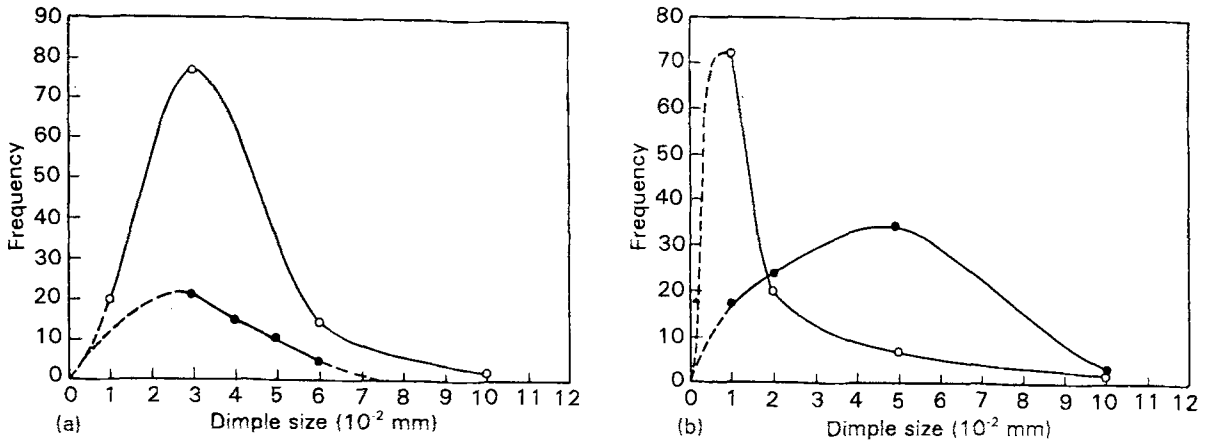

Figure 13 The statistical distributions of dimple size for the two notch geometries under different loading conditions. (a) Dimple size distributions for the semi-circle notch configuration, (○) + 6000, − 3000 kgf, (●) + 4000, − 4000 kgf. (b) Dimple size distributions for the V-notch configuration, (○) + 6000, − 3000 kgf, (●) + 4500, − 4500 kgf.

TABLE IV The relationships between both the maximum cyclic force, F_{max}, and the mean stress, σ_m, and the fatigue fracture surface features, namely the ratio of the fibrous area diameter (dl)/total area diameter (D), strain width (W) and the dimple size (d)

Correlation parameters	Notch geometry	Best regression function	
F_{max} (kgf) dl/D	(a) Semi-circle	$F_{max} = 2838.19 + 5757.41[(dl/D) - 0.35]/0.45) - 1209.57[(dl/D) - 0.35] - 0.35/0.45^2$	(18)
	(b) V-notch	$F_{max} = 652.57 + 11\,626.39[(dl/D) - 0.35]/0.45 - 5151.16[(dl/D) - 0.35]/0.45^2$	(19)
σ_m (MPa) dl/D	(a) Semi-circle	$\sigma_m = 1676.6[(dl/D) - 0.5]/0.3 - 2626.56[(dl/D) - 0.5]/0.3^2 + 1474.87[(dl/D) - 0.5]/0.3^3 - 180$	(20)
	(b) V-notch	$\sigma_m = 4863.38[(dl/D) - 0.5]/0.3 - 7789.71[(dl/D) - 0.5]/0.3^2 + 4092.21[(dl/D) - 0.5]/0.3^3 - 820$	(21)
F_{max} (kgf) W (mms)	(a) Semi-circle	$F_{max} = 5826.287 - 107\,021.3046(W/0.016) + 1851\,028.87(W/0.016)^2 - 10\,594\,031(W/0.016)^3 + 20\,262\,776(W/0.016)^4$	(22)
	(b) V-notch	$F_{max} = 3925.78 + 1251(W/0.016) - 2383.4(W/0.016)^2 + 8722.036(W/0.016)^3 - 4025.066(W/0.016)^4$	(23)
σ_m (MPa) W (mms)	(a) Semi-circle	$\sigma_m = 48.64 + 242.71(W/0.015) + 2489.75(W/0.015)^2$	(24)
	(b) V-notch	$\sigma_m = 87.147 - 31.96(W/0.015) + 232.68(W/0.015)^2$	(25)
F_{max} (kgf) d (mms)	(a) Semi-circle	$F_{max} = 7144.96 - 9839.4355(d/0.08) + 117\,555.89(d/0.08)^2 - 5501.734(d/0.08)^3$	(26)
	(b) V-notch	$F_{max} = 6586.70 - 22\,338.73(d/0.08) + 29\,581.95(d/0.08)^2$	(27)
σ_m (MPa) d (mms)	(a) Semi-circle	$\sigma_m = 257.645 - 751.218(d/0.77) + 797.54(d/0.07)^2 - 332.72(d/0.07)^3$	(28)
	(b) V-notch	$\sigma_m = 257.9905 - 1593.16(d/0.07) + 2253.02(d/0.07)^2$	(29)

surface features, specifically the average dimple diameter and the dimple size distributions, on both the maximum cyclic loads and the mean stress for the two notch configurations are consequently presented in Figs 12 and 13. The dimple size decreases upon decreasing either the cyclic maximum applied stress or the mean stress levels. The trends for the semi-circle notch are generally higher than those trends for the V-notch geometry. It is interesting to report that the dimple size distribution for the semi-circle notch reveals a statistical peak corresponding to a dimple size of about 0.3 mm and does not depend on the mean stress level, while the dimple size corresponding to the maximum statistical occurrence for the V-notch changes from about 0.015 mm to 0.05 mm upon changing the mean stress levels.

An attempt was made through extensive sensitivity and regression analysis to correlate the fracture surface features with the loading conditions, specifically the maximum applied cyclic loads and the mean stress levels. This approach can be adopted and established to estimate the applied cyclic loading conditions from the measurements of the fracture surface features which is of prime importance for design and failure analysis and diagnosis of engineering components. A summary of these types of correlations are given in Table IV.

The difference in the characteristic features in both the fatigued area as well as the ductile fracture region in the two types of notches, is mainly related to the difference in the strain fields under different applied stresses for each notch. These different strains demonstrate the notch geometry response to the ductility of AISI 304 stainless steel. It is worth pointing out that the plastic deformation prior to fracture is controlled by the formation and subsequent shrinking of dislocations cells [17] which, as strain is increased, extend past grain boundaries. Thus, it can be deduced that the small voids or dimples formed in the V-notch specimens are due to the presence of large numbers of nucleation sites, unlike inclusion distributions which are related to the presence of highly stressed regions due to the formation of dislocation structures in the uniform strain region. Because notches do not, in general, exhibit a uniform strain region during fracture, voids due to dislocation mechanisms, as well as void nucleation due to decohesion of large inclusions, appear to be the dominant features of the fracture process in the present study.

4. Conclusions

A comparison of the monotonic and cyclic curves for AISI 304 stainless steel indicated that this steel possesses a remarkable cyclic hardening phenomenon. The elastic–plastic low-cycle fatigue investigation reported in the present study indicates the paramount effects of the maximum stress, the mean stress and the notch geometry on the fatigue life as well as the fatigue behaviour process. Establishment of the macroscopic fatigue parameter is conducted through careful sensitivity and regression analysis. Finally, extensive scanning electron microscopic observation of the fracture surfaces of both semi-circle and V-notch configuration under different cyclic loading conditions revealed a large dependence of the microscopic features upon the macroscopic parameters and an attempt was comprehensively made to correlate the ratio of the fibrous area to the total area, the striation width and the dimple size, as well as the dimple distributions, with the maximum stress and the mean stress for both semi-circle and V-notch geometry, this leads to the suggestion that the dislocation mechanisms, as well as the decohesion of large inclusions combined are the dominant features of void nucleation and fatigue behaviour in AISI 304 stainless steel.

References

1. M. R. BAYOUMI, *Bull. Fac. Assiut Univ.* **16** Part (I) (1988) 115.
2. *Idem, ibid.*, **16**(2) (1988) 121.
3. J. J. BURKE and V. WEISS, in "Fatigue Environment and Temperature Effects" (Plenum, New York, 1983) pp. 241–61.
4. C. R. BRINKMAN, G. E. KORTH and R. R. HOBBINS, *Nucl. Technol.* **16** (1972) 297.
5. R. HALES and B. TOMKINS, "Creep Fatigue Failure in Austenitic Stainless Steels Relevant to Structural Performance", PVP-70, Paper 82 (American Society of Mechanical Engineers, New York, 1982).
6. L. F. COFFIN, in Fatigue and Microstructure", edited by M. Meshii (American Society for Metals, Metals Park, OH, 1979) pp. 1–12.
7. M. R. MITCHELL, *ibid.*, pp. 385–95.
8. A. FRANKE, J. KRATOCHVIL, M. SAXLOVA and R. SEDLACEK, *Mater. Sci. Eng. A Struct. Mater. Prop. Microstruct. Process.* **A 137** (1991) 119.
9. D. KUHLMAN-WILDSDOFR and N. HANSEN, *Metall. Trans.* (1989) 2393.
10. J. F. KNOTT, "Fundamentals of Fracture Mechanics" (Halsted Press, New York, 1973).
11. O. BUXBAUM, H. KLATSCHKE and H. OPPERMANN, *Rev.* **44** (1991) 27.
12. M. A. ERICKSON, MSc Thesis, University of Virginia, Charlottesville, VA (1983).
13. M. N. BASSIM, R. J. KASSEN, M. R. BAYOUMI and H. G. F. WILSDORF, *J. Mater. Sci. Eng.* **91** (1987) 107.
14. A. S. ARGON, J. IM and R. SAFOGLU, *Metall. Trans.* **62** (1975) 825.
15. S. H. GOODS and G. M. BROWN, *Acta Metall.* **27** (1979) 442.
16. R. J. KLASSEN, MSc Thesis, University of Manitoba, Winnipeg, Manitoba, Canada (1986).
17. M. R. BAYOUMI, in "Proceedings of the Second International Ain-Shams University Conference on Production Engineering and Design for Development", Cairo, Egypt, Vol. 2, (1987) pp. 289–97.

Received 15 May 1992
and accepted 26 February 1993